Spin-flip Raman scattering from donor-bound electrons in $Cd_{1-x}Mn_xTe/Cd_{1-y}Mg_yTe$ single quantum wells

R. Meyer, M. Dahl,* G. Schaack, and A. Waag

Physikalisches Institut der Universität Würzburg, Am Hubland, D-97074 Würzburg, Germany

(Received 6 December 1996)

We report on the spin-flip Raman scattering of electrons bound to shallow donors in single quantum wells of $Cd_{1-x}Mn_xTe$ between $Cd_{1-y}Mg_yTe$ barriers. An enhancement of the scattering intensity of the bound magnetic polaron was found for narrow quantum wells. A variational treatment of the quantum well exciton in combination with the polaron model developed for bulk material is applied to interpret the experimental observations. The reduced symmetry of the quantum well states manifests itself through the observation of new resonances in the Raman scattering cross section. A simple model taking into account the anisotropy of the Zeeman effect of the valence band can reproduce the observations. [S0163-1829(97)00724-8]

I. INTRODUCTION

Since the first observations of spin-flip Raman scattering (SFRS) in InSb (Ref. 1) and CdS,[2] there has been a strong interest in this effect as a tool to study intrinsic properties (g factors and band parameters) of electrons and holes in semiconductors. Reviews were given by Scott,[3] Geschwind and Romestain,[4] and Häfele.[5] More recently spin-flip transitions of holes in $GaAs/Ga_{1-x}Al_xAs$ quantum well structures were observed.[6,7] The method has also been applied to investigate p-type doping in wide band gap II-VI materials.[8,9]

Diluted magnetic semiconductors (DMS's) are semiconductors where cations are substituted by magnetic ions, e.g., $Cd_{1-x}Mn_xTe$. This class of alloys also called semimagnetic semiconductors is especially well suited for SFRS studies since the Zeeman splitting of the band states is extremely large due to the strong exchange interaction between the free carriers and the magnetic ions.[10] SFRS experiments on bulk DMS's allowed a direct determination of the conduction band exchange constant, and it also revealed the existence of a bound magnetic polaron (BMP), where a donor-bound electron and magnetic ions form a ferromagnetically ordered cluster.[11–14] SFRS studies of highly doped materials allow us to determine spin relaxation times T_2 and spin diffusion coefficients of itinerant electrons.[15,16] Analysis of the resonance enhancement of SFRS near the E_0 band edge in bulk $Cd_{1-x}Mn_xTe$ revealed donor-bound excitons as intermediate states in the scattering process.[17] SFRS from heterostructures containing DMS layers and quantum dots were reported.[18–22] As the spin flip (SF) of electrons confined to quantum wells (QW's) is very sensitive to the overlap of the electron envelope function and the DMS material, it provides a means to probe the distribution of the magnetic ions. From the study of the resonance profiles it is also possible to deduce information on the binding energy and distribution of donors in QW structures.[21]

In this paper we report on the observation of SFRS in single quantum wells (SQW's) of $Cd_{1-x}Mn_xTe$ with $Cd_{1-y}Mg_yTe$ as barriers. Evidence for an enhancement of the BMP energy for donor-bound electrons in narrow QW's is given and discussed as an effect of the QW confinement.

The occurrence of resonances in the SFRS scattering cross section for QW structures which are forbidden in bulk material is shown and interpreted as a consequence of the reduced symmetry of a QW structure compared to bulk material. A preliminary account of some of these results has been already given in Ref. 23. Here we will discuss in more detail the selection rules of SFRS in a QW and give a more extensive description of the model calculation.

II. EXPERIMENT

The $Cd_{1-x}Mn_xTe/Cd_{1-y}Mg_yTe$ SQW's were grown by molecular beam epitaxy (MBE) on $Cd_{1-z}Zn_zTe$ substrates ($z = 0.03$) with a (001) orientation. The zinc content was chosen to match the lattice constant of the barrier material. The general layout of the samples consisted of a thick buffer layer on top of the substrate followed by a series of different wells. The latter being separated by thick barriers thus providing a situation where the electronically isolated wells are strained and the barriers are almost free of strain. No intentional doping of the structures was performed, however, from the excitation power dependence of the SFRS intensity we deduce the occurrence of residual donors. Table I gives a compilation of important sample parameters. The large depth of the conduction and valence band potential wells, $V_{cb} = 261$ meV and $V_{vb} = 112$ meV for sample CT669, provide a strong confinement of electron and holes for these type-I QW structures. For the valence band offset we assume a value $Q_{vb} = 0.30$ which has been determined for (Cd,Mn)Te and (Cd,Mg)Te.[24,25]

For the light scattering experiments the sample was placed in a superconducting split-coil magnet providing fields $B \leq 7.5$ T and temperatures 1.7 K$< T < 100$ K. Voigt backscattering geometry, i.e., propagation direction of the incident $\vec{k}_i$ and scattered $\vec{k}_s$ light normal to the (001) plane and the field direction along [100], was applied. A cylindrical focussing lens was used to keep the power density below ≈ 1 $W cm^{-2}$. An argon ion laser- pumped dye laser (pyridine and DCM) served as a tunable light source. The spectral analysis and detection of the scattered light was done using a triple spectrograph (DILOR XY, $f = 0.50 m$) equipped with a

TABLE I. Sample parameters of the $Cd_{1-x}Mn_xTe/Cd_{1-y}Mg_yTe$ single quantum well structures. Concentrations and thicknesses as determined from the growth process.

Sample	x	y	L_z (Å)	Barrier (Å)	Buffer (Å)
CT669	0.03	0.24	18, 45, 60, 100	500	2000
CT671	0.075	0.29	18, 45, 100	500	2000
CT716	0.10	0.37	6, 18, 45, 100, 300	500	2000

liquid nitrogen-cooled CCD camera. The double monochromator filter of the triple spectrograph and standard photon counting equipment were applied to take the photoluminescence excitation (PLE) spectra.

III. DONOR-BOUND MAGNETIC POLARONS IN QUANTUM WELLS

A. Experimental results

Typical Raman spectra of a SQW $Cd_{0.93}Mn_{0.07}Te/Cd_{0.71}Mg_{0.29}Te$ sample are shown in Fig. 1. The two spectra differ in the orientation of the polarization of the incident light which was either parallel (π) or normal (σ) to the direction of the magnetic field. The scattered light was analyzed normal to the field direction for both spectra. A strong spin-flip Raman line is only visible in the ($\pi\sigma$) spectra where polarization and analyzation are orthogonal (crossed polarization). The weak line in the ($\sigma\sigma$) spectra is caused by a lack of perfect polarizations mainly introduced by depolarization due to cryostat windows. The other excitations visible in the spectra are the CdTe-like and the MnTe-like LO phonons and a replica of the internal SF of an electron in the $Mn^{2+}3d$ shell associated with the CdTe-like LO phonon.[26]

The magnetic field dependence of the Raman shift related to the spin-flip excitation of donor-bound electrons of sample CT669 is shown in Fig. 2 for electrons confined to four wells of nominal thicknesses $L_z=18$ Å, $L_z=45$ Å, $L_z=60$ Å, and $L_z=100$ Å. The shift displays the well known saturation behavior, roughly following a Brillouin function $\mathcal{B}_{5/2}(\eta)$. The high-field Raman shifts decrease with decreasing well thickness, consistent with the penetration of the electron-wave function into the nonmagnetic (Cd,Mg)Te barriers. Similar observations have been made for (Cd,Mn)Te/ZnTe multiquantum well structures.[27] The situation is more complex in the low-field limit where the BMP effect has to be considered. According to Dietl and Spałek[28] the peak position $\widetilde{\Delta}$ of Stokes SFRS can be described by the following equation:

$$\widetilde{\Delta}^2 - 2\varepsilon_p\widetilde{\Delta} - \widetilde{\Delta}\Delta_0 \coth\left(\frac{\widetilde{\Delta}\Delta_0}{4\varepsilon_p k_B T}\right) - 4\varepsilon_p k_B T = 0, \quad (1)$$

where ε_p is the characteristic polaron energy as defined in Ref. 28. It is related to the characteristic energy parameter W_0 used by Heiman et al.:[12]

$$\varepsilon_p = \frac{3}{14}\frac{\frac{5}{2}W_0^2}{k_B(T+T_0)}\frac{\partial}{\partial\eta}\mathcal{B}_{5/2}(\eta) \approx \frac{W_0^2}{4k_B(T+T_0)}, \quad \eta \ll 1$$

$$\eta = \frac{\frac{5}{2}g\mu_B B}{k_B(T+T_0)}. \quad (2)$$

To include the influence of the QW we modify the valence band spin splitting Δ_0 by introducing a factor P_w,

$$\Delta_0 = P_w \bar{x}\alpha N_0 \frac{5}{2}\mathcal{B}_{5/2}(\eta) + g^*\mu_B B. \quad (3)$$

P_w is the probability of finding the electron inside the semimagnetic well. P_w was calculated for $B=0$ T within a simple envelope approximation. All other symbols have their usual meanings: αN_0 is the sd exchange energy, N_0 the density of cation sites, and g_{Mn} and g^* are the Mn^{2+} and the valence band g factors. $\bar{x}$ and T_0 are two empirically introduced parameters that allow us an approximate description of the total magnetization of the coupled Mn^{2+} ion system by a Brillouin-type function. The parameter $\bar{x} \leq x$ takes into account the reduction of the average spin per ion due to antiferromagnetically coupled clusters.[29] For small x values the dominant reduction is due to nearest neighbor (NN) pairs which have an $S=0$ ground state. T_0 is mainly determined by the interaction with neighbors beyond the NN distance. The product $\bar{x}N_0\alpha, T_0$, and W_0 were used as parameters in a least squares fit of Eqs. (1), (2), and (3) to the data. The fitted Raman shifts are plotted as solid lines in Fig. 2. Results for the fit parameters are tabulated in Table II. A high background due to photoluminescence and Rayleigh scattering prevented the determination of data in the low-field region for the $L_z=45$ Å well of sample CT669. Therefore no significant values for W_0 and T_0 could be fitted in this case. The most interesting results in Table II are the large values for W_0. For the narrow wells they exceed the values for the bulk material of the same Mn content considerably. This aspect will be the subject of the following subsection.

With $N_0\alpha=220$ meV (Ref. 29) the values for $\bar{x}N_0\alpha$ in Table II lead to effective Mn concentrations that correspond well with the x values from the growth process for sample CT669 and CT716 while for CT671 the value $\bar{x}=0.043$ suggests a Mn content $x \approx 0.11$ which is distinctly higher than intended in the growth process. Using this higher value of x for sample CT671 we give the fraction of magnetically active Mn^{2+} ions $\bar{x}/x$ in Table II. The value of x for sample CT671 is also supported by the high values for T_0.

The inset of Fig. 2 shows the SF Raman shift for the four wells of sample CT669 at a field $B=7.0$ T versus the calculated probability P_w. Assuming a saturation of the Brillouin function, which is reasonable for the low temperature and low Mn content, a straight line fit, according to Eq. (3), yields a value $\bar{x}N_0\alpha=4.2\pm0.4$ meV. The result for the intrinsic CdTe g factor derived from the straight line fit is rather uncertain $g^*=-2.6\pm2.0$, however, in agreement with the literature value $g^*=-1.77$.[30] The good linearity and reasonable values for $\bar{x}N_0\alpha$ and g^* show that the use of a simple QW model neglecting interface effects and changes of P_w with magnetic field are reasonable approximations for the low x values and deep wells of our samples.
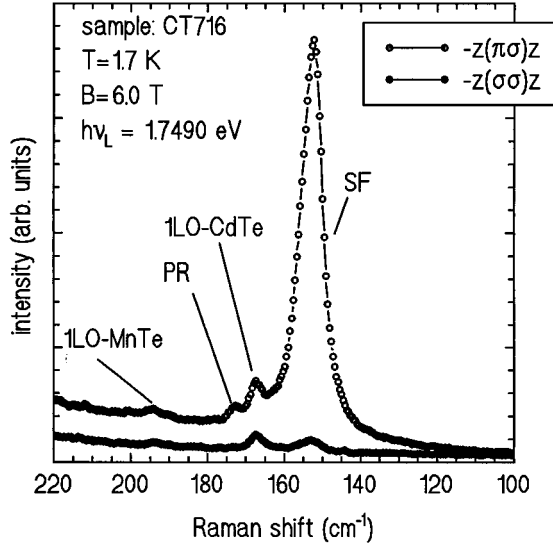
FIG. 1. Raman spectra in crossed ($\pi\sigma$) and parallel ($\sigma\sigma$) polarization for a $Cd_{0.9}Mn_{0.1}Te/Cd_{0.63}Mg_{0.37}Te$ single quantum well of width $L_z = 100$ Å. Incident and scattered light propagate along the growth axis [001] while the magnetic field is in [100] direction. PR: paramagnetic resonance of the Mn^{2+} ion ($3d^5$) as a companion ($\Delta = 5.6$ cm^{-1}) of the 1LO-CdTe phonon mode Ref. 26.

B. Model for BMP enhancement

While for the free magnetic polaron reduction of the dimension has an important influence on the localization and therefore on the polaron formation,[31] for the BMP the localization is provided by the defect potential and we expect that the reduction in dimensionality caused by the QW should only have an indirect influence on the BMP. We therefore use the BMP model derived for bulk materials since the thermodynamic properties of the BMP should not be affected by the QW potential. We adopt the result derived by Wolff[14]

$$W_0^2 = \frac{35}{12}\bar{x}(N_0\alpha)^2 \int \frac{|\Phi(r)|^4 d^3r}{N_0}, \qquad (4)$$

which expresses the characteristic polaron energy W_0 in terms of the effective Mn concentration, exchange energy, and the donor wave function $\Phi(r)$. The use of a $1S$ hydrogenic function $\Phi(r) = (\pi a_0^3)^{-1/2}\exp(-r/a_0)$ for bulk material leads to the result

FIG. 2. Magnetic field dependence of the spin-flip Raman shift for donor-bound electrons confined to four single quantum wells of a $Cd_{0.97}Mn_{0.03}Te/Cd_{0.76}Mg_{0.24}Te$ sample. Solid lines are fits to the BMP model (see text). Inset: Saturation value of the Zeeman splitting versus the calculated probability P_w of finding the electron of the first subband within the potential well.

$$W_0^2 = \frac{35}{96}\frac{\bar{x}(N_0\alpha)^2}{\pi N_0 a_0^3}. \qquad (5)$$

Heiman et al.[12] showed that Eq. (5) is in agreement with the experiment for bulk (Cd,Mn)Se.

If we neglect interface effects on the effective Mn concentration $\bar{x}$, which is reasonable for low Mn content and structures with semimagnetic well material, the influence of the QW on W_0 is mainly through the donor wave function. It is well known that the additional localization due to the QW leads to an increase of the donor binding energy as long as

TABLE II. Parameter derived from fitting the BMP model to the SFRS data for several $Cd_{1-x}Mn_xTe/Cd_{1-y}Mg_yTe$ single quantum wells.

Sample	L_z (Å)	P_w	$\bar{x}N_0\alpha$ (meV)	W_0 (meV)	T_0 (K)	$\frac{\bar{x}}{x}$
CT669	18	0.63	4.3±0.3	0.27±0.15	2.6	0.65
CT669	45	0.89	4.4±0.3			0.67
CT669	65	0.95	4.4±0.2	0.36±0.15	2.8	0.67
CT669	100	0.98	4.4±0.2	0.00±0.15	2.6	0.67
CT671	≈ 20	0.60	9.5	0.94±0.2	3.5	0.39
CT671	100	0.98	9.4±0.3	0.34±0.2	3.6±0.4	0.39
CT716	45	0.92	9.2	0.79±0.2	4.4	0.42

TABLE III. Material parameters for (Cd,Mn)Te and (Cd,Mg)Te used for the calculations. Parameters not known for (Cd,Mg)Te were replaced by the values for (Cd,Mn)Te and vice versa.

	Unit	$Cd_{1-x}Mn_xTe$	Source	$Cd_{1-y}Mg_yTe$	Source
Band gap	meV	$E_0 = 1596 + 1605\,x$	Ref. 41	$E_0 = 1598 + 1755\,y$	Ref. 40
Eff. mass	m_0	$0.096(x=0)$	Ref. 42		
Luttinger param.		$\gamma_1 = 4.14, \gamma_2 = 1.09$	Ref. 43		
Static dielectr. const.		$\varepsilon_0 = 9.65(x=0)$	Ref. 43	$\varepsilon_0 = 10.76 - 3.86y$	Ref. 44
vb offset		$Q_{vb} = 0.3$	Ref. 25	$Q_{vb} = 0.3$	Ref. 24

the donor wave function does not penetrate significantly into the barrier. The latter happens in very narrow wells where the bulk situation is approached and for donors located near the interface or in the barrier. In the latter case the binding energy can be reduced below the bulk value, depending on the donor position z_i and barrier height V_b. The increase or reduction in binding energy is accompanied by a shrinking or expansion of the extension of the donor wave function which affects the BMP.

A standard approach to the problem of the donor in a QW is a variational treatment. Since we are only interested in the major trends for the BMP in a QW we use the simplest trial function

$$\Phi(r) = \chi(z)\phi(\varrho) = \chi(z)\sqrt{\frac{2}{\pi}}\frac{1}{a_0^{2D}}\exp(-\varrho/a_0^{2D}). \quad (6)$$

$\chi(z)$ is the conduction band envelope function of the ground state and $\phi(\varrho)$ is a two-dimensional $1S$ hydrogenic wave function, with $\varrho = \sqrt{x^2 + y^2}$ being the variable for the electron motion in the QW plane. The application of this separable trial function simplifies the solution of the variational problem and leads to a straightforward numerical problem (see, e.g., Ref. 32). As a result of the variational procedure one gets the energy and 2D Bohr radius for the donor depending on the position of the donor z_i. In Table III we give the parameters (band gaps, band offset, . . .) used in the calculation.

Inserting wave function (6) for the donor into Eq. (4) leads to a characteristic energy W_0^{QW} in a QW structure of the form

$$(W_0^{QW}(z_i))^2 = \frac{35}{24}\frac{\bar{x}(N_0\alpha)^2}{\pi(a_0^{2D}(z_i))^2}\int_{-L/2}^{+L/2}\frac{|\chi(z)|^4}{N_0}dz, \quad (7)$$

where the argument z_i indicates the dependence on donor position. This expression is easily evaluated once the variational problem has been solved. However, there are additional problems that complicate the comparison with the experiment. First, since our samples are not intentionally doped we do not know the distribution of the donors along the growth axis. Second, the experiments are performed under resonance condition, which leads to weighted contributions of donors to the signal due to the resonance enhancement. To get an estimation of the influence of the donor position we consider three situations: (i) donor in the center of the well, (ii) donor at the interface between well and barrier, and (iii) donors equally distributed over the well. Figure 3 shows the calculated curves for the three sample structures together with the experimental results. (Due to the identical values

$\bar{x}N_0\alpha$ and the large depth of the wells, the theoretical curves for sample CT671 and CT716 do not differ significantly. For reasons of clarity only one set of theoretical curves is displayed in Fig. 3.) For samples CT671 and CT716 the observed and calculated values for W_0 are at least in qualitative agreement. The increasing trend in W_0 with reduction of the well thickness is reproduced by the calculation.

The situation is less clear for sample CT669. Here for the two narrow QW's with $L_z = 65$ Å and $L_z = 20$ Å a BMP is observed and the W_0 values agree or almost agree with the calculation, while the wide well with $L_z = 100$ Å shows almost no detectable BMP. A possible explanation could be a distribution of the donors which has a maximum in the barrier near the interface to the well. In this case the donor binding energy for a wide well is reduced below the bulk value, but for narrow wells an enhanced donor binding would still be possible.

For future experiments the use of δ doped samples could avoid such ambiguities. Also samples with a constant Mn content along the growth axis like $Cd_{1-x}Mn_xTe/Cd_{1-x-y}Mn_xMg_yTe$ would be very interesting since the part
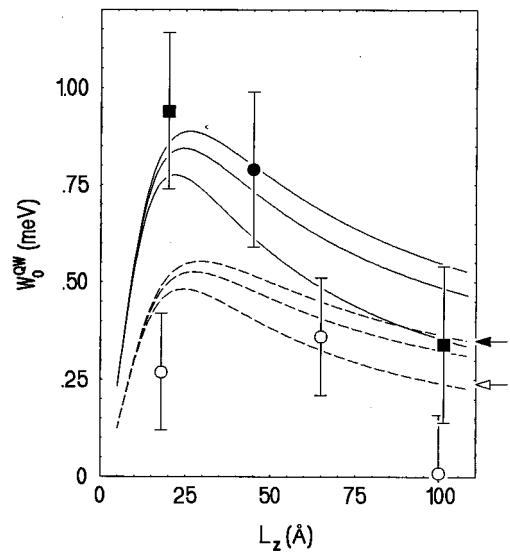
FIG. 3. Experimental and calculated characteristic polaron energies for three $Cd_{1-x}Mn_xTe/Cd_{1-y}Mg_yTe$ structures. Solid lines and solid marks correspond to samples CT671 (■) and CT716 (●) and dashed lines and open circles to sample CT669 (○). The upper (lower) calculated curve corresponds to the center (interface) position of the donors. The intermediate curve is calculated for donors that are equally distributed within the well. The arrows mark the bulk values calculated with Eq. (5).
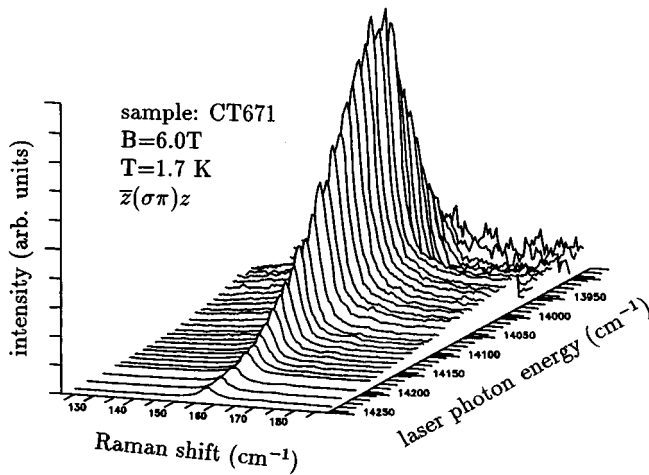
FIG. 4. Spin-flip Raman spectra for a $Cd_{1-x}Mn_xTe/Cd_{1-y}Mg_yTe$ single quantum well ($L_z = 100$ Å) for several excitation energies chosen around a resonance of the scattering cross section.

of the wave function penetrating into the barrier would still contribute to the BMP energy and such samples would also avoid interface effects on the effective Mn concentration.

IV. RESONANCE OF THE SPIN-FLIP RAMAN SCATTERING IN QUANTUM WELLS

A. Experimental results

The intensity of the SFRS signals shows a strong dependence on the quantum energy of the exciting light, as has been observed earlier.[19,21] An example for the SF excitation in the $L_z = 100$ Å well of sample CT671 is shown in Fig. 4, where a series of spectra differing in excitation energy is displayed. A more concise description of the information contained in Fig. 4 is given by a resonance profile, extracted from such a series of data, where the integral scattering intensity of a Raman line versus the energy of the incident photon energy is plotted. In Fig. 5 the resonance profiles for the $z(\sigma\pi)\bar{z}$ and $z(\pi\sigma)\bar{z}$ scattering geometries are shown for transitions of the $L_z = 45$ Å QW of sample CT669.

Three different resonances are clearly resolved in Fig. 5. A fourth resonance is indicated at the low energy side of the $(\pi\sigma)$ profile. The full resonance is not accessible to the experiment because of the strong luminescence at the band edge. The occurrence of four resonances is different from the situation in (Cd,Mn)Te bulk material where only two resonances involving light-hole excitonic transitions are observed.[17]

For the identification of the transitions involved in the Raman resonance the knowledge of the PLE spectra is very helpful. We show in Fig. 6 the PLE spectra detected at the low-energy side of the band edge luminescence for the $L_z = 45$ Å well and two polarizations of the emitted light. The spectra were taken under identical conditions of field and temperature as the Raman data. Several maxima are visible and we relate them with the absorption due to free excitons associated with the different Zeeman-split components of the lowest subbands of the QW. We discuss the identification of the individual transitions below.
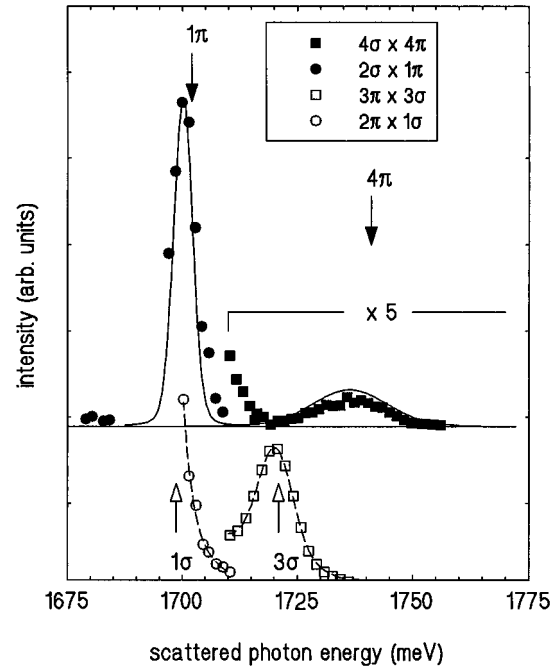
FIG. 5. Resonance profiles for the spin-flip Raman scattering from a $Cd_{0.97}Mn_{0.03}Te/Cd_{0.24}Mg_{0.76}Te$ single quantum well. The various resonances are labeled with a consecutive number and polarization of the incident and scattered photon. The arrows mark the transition energy as determined by PLE.
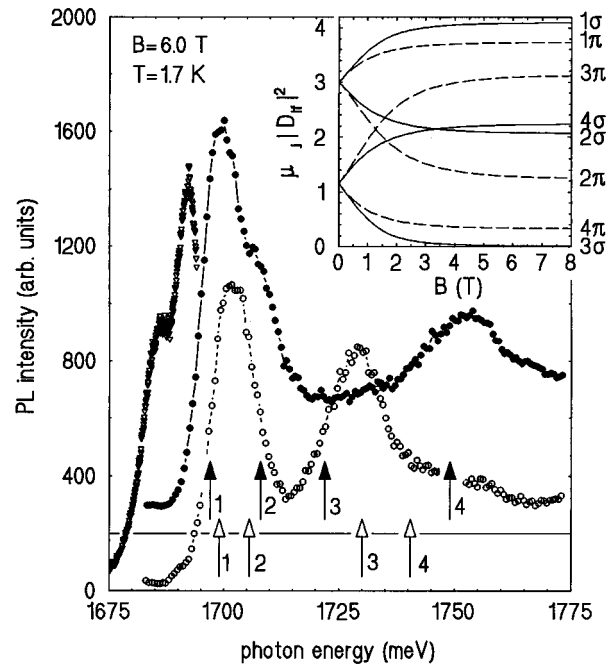
FIG. 6. Photoluminescence spectrum ($\triangleleft$) and photoluminescence excitation spectra for $\sigma(\bullet)$ and $\pi(\bigcirc)$ analyzation for a $Cd_{0.97}Mn_{0.03}Te/Cd_{0.24}Mg_{0.76}Te$ single quantum well. Open and solid arrows give the position of the calculated dipole transitions, respectively. The inset shows the calculated magnetic field dependence of the relative absorption strength for the eight dipole transitions.

B. Interpretation of the resonance behavior

When comparing Raman scattering of bulk material and QW structures one expects the symmetry reduction to manifest itself in relaxed selection rules. If we include the magnetic field the point symmetry appropriate for bulk CdTe material is S_4, assuming the B field to be parallel to a fourfold axis. For the QW structure which has point symmetry D_{2d} in the zero field two situations are of interest: (I) magnetic field parallel to the growth direction [001], (II) magnetic field normal to the growth direction along [100] or [010]. The first case leads to symmetry group S_4 and thus to identical selection rules as for bulk material. In the second case the symmetry group is reduced to C_2 [Fig. 7(a)].

A general selection rule for magnetic excitation (in monoclinic or higher symmetries)[33] requires that the incident light has a polarization component ($\vec{\varepsilon}_i$) parallel to the magnetic field ($\vec{\varepsilon}_B$) while the scattered light ($\vec{\varepsilon}_s$) is polarized normal to $\vec{B}$ or vice versa, in short, $\vec{\varepsilon}_B \times \vec{\varepsilon}_i \times \vec{\varepsilon}_s \neq 0$. Observation of spin-flip excitations in geometries corresponding to situation (I) are therefore practically impossible, since this would require a backscattering experiment with the light traveling along the well plane or a 90° scattering geometry, where either scattered or incident light travels along the plane of the QW. Both experiments are not feasible with reasonable accuracy by standard Raman techniques. SFRS in geometries corresponding to situation (II) is however easily realized in a Voigt backscattering configuration.

In Fig. 7(a) we show a schematic diagram of the splitting of the conduction and valence subband at the Brillouin zone center for fields $B\|[001]$ and $B\|[100]$. The most obvious consequence of the reduced symmetry caused by the in plane field is the fact that the Stokes and the anti-Stokes spin-flip transition transform according to the same irreducible representations Γ_2 of C_2, i.e., $\Gamma_3^* \times \Gamma_4 = \Gamma_4^* \times \Gamma_3 = \Gamma_2$, while in the (bulk) symmetry S_4 the two excitations belong to different, Kramers conjugate irreducible representations $\Gamma_6^* \times \Gamma_5 = \Gamma_3$ and $\Gamma_5^* \times \Gamma_6 = \Gamma_4$. The latter allows us by a suitable choice of the scattering geometry to observe Stokes and anti-Stokes Raman lines in different spectra, as has been shown in Ref. 13. This separation of Stokes and anti-Stokes lines should be suppressed in the C_2 symmetry; however, the experimental verification of this result also requires a 90° scattering geometry and could therefore not be observed.

The existence of four resonances in the Raman cross section for $B\|[100]$ follows also from Fig. 7(a). The magnetic field splits each heavy-hole and light-hole state into a Γ_3 and a Γ_4 state. The distinction between heavy and light hole is thus obsolete and eight electric-dipole transitions between the valence and the conduction band, with polarizations as shown in Fig. 7(a), are allowed.

Spin-flip Raman scattering can be described by the second order perturbation theory, which leads to the following cross section:[33]

$$\frac{d\sigma}{d\Omega} \propto \left| \sum_l \frac{\langle f|\vec{e}_S^* \vec{D}|l\rangle \langle l|\vec{e}_I \vec{D}|i\rangle}{E_i - E_l + \hbar\omega_I} + \frac{\langle f|\vec{e}_I \vec{D}|l\rangle \langle l|\vec{e}_S^* \vec{D}|i\rangle}{E_i - E_l - \hbar\omega_S} \right|^2 , \tag{8}$$

where $|i\rangle, |l\rangle$, and $|f\rangle$ are the initial, intermediate, and final state of the scattering process and E_i, E_l, and E_f are the

corresponding energies. $\vec{D}$ is the dipole operator, $\vec{e}_I$ and $\vec{e}_S$ the polarization vectors of the incident and scattered light, $\hbar\omega_I$ and $\hbar\omega_S$ are the corresponding photon energies. Only the first term in Eq. (8) shows resonance behavior and we will consider only such terms in the following. The eight dipole transitions in Fig. 7(a) can be combined to four Stokes Raman processes, two corresponding to ($\pi\sigma$) and two corresponding to ($\sigma\pi$) polarization. For $B\|[001]$ the magnetic field does not lift the distinction between heavy and light holes, thus like in bulk material only six electric-dipole transitions and two Raman processes are allowed.

To support our identification of the resonances we performed a simple model calculation of the Zeeman splitting of QW states in an in plane field. This problem has been treated in a more general way in the literature.[34–37] Since we are only interested in samples where the Zeeman shift is small compared to the depth of the QW we treat the exchange interaction as a perturbation to the QW problem. For a system with semimagnetic well material we write within the virtual-crystal and mean-field approximation,[38]

$$H_{ex}^{cb} = -xN_0\alpha\langle S\rangle s_i^e \Theta\left(\frac{L_z^2}{4} - z^2\right), \tag{9}$$

$$H_{ex}^{vb} = -xN_0\beta\langle S\rangle s_i^h \Theta\left(\frac{L_z^2}{4} - z^2\right), \tag{10}$$

for the exchange terms. $\Theta(z)$ is the unit-step function, $N_0\beta$ is the pd exchange energy and $s_i^e(s_i^h)$ is the component of the angular momentum operator of the band electron (hole) along the magnetic field direction, i.e., $s_x^e(s_x^h)$ for $B\|[100]$. We diagonalize H_{ex}^{cb} within the subspace of the spin degenerate lowest conduction subbands and H_{ex}^{vb} within the four-dimensional space of the lowest heavy- and light-hole subbands. We are only interested in the band edge energies and neglect the in plane dispersion terms. With $k_\perp^e = k_\perp^h = 0$ the conduction and valence band matrices for $B\|[100]$ take the following form:

$$H^{cb} = \begin{pmatrix} 0 & 3CP_{56} \\ 3CP_{65} & 0 \end{pmatrix},$$

$$C = -\frac{1}{6}\bar{x}N_0\alpha\frac{5}{2}\mathcal{B}_{5/2}(\eta), \tag{11}$$

$$H^{vb} = \begin{pmatrix} 0 & \sqrt{3}C'P_{12} & 0 & 0 \\ \sqrt{3}C'P_{21} & \Delta & 2C'P_{23} & 0 \\ 0 & 2C'P_{32} & \Delta & \sqrt{3}C'P_{34} \\ 0 & 0 & \sqrt{3}C'P_{43} & 0 \end{pmatrix},$$

$$C' = -\frac{1}{6}xN_0\beta\frac{5}{2}\mathcal{B}_{5/2}(\eta), \tag{12}$$

where the energy of the heavy hole for $B = 0$ T is taken as zero and Δ is the light hole-heavy hole splitting due to the QW potential and the strain. The Mn concentration x and the spin expectation $\langle S\rangle$ value have been replaced by the effective Mn concentration and the Brillouin function. The factors P_{ij} are defined by

$$P_{ij} = \int_{-L/2}^{+L/2} \chi_i^*(z) \chi_j(z) dz, \qquad (13)$$

with $\chi_i(z)$ being the envelope functions. A unitary transformation leading to a bloc-diagonal form for Eq. (12) is easily found. The resulting two-by-two matrices correspond to the two irreducible representations Γ_3 and Γ_4 of the point group C_2 and the eigenvalues can be found analytically. The results are however lengthy and we do not reproduce the expressions here. As an example for the Zeeman splitting in in plane fields we show in Fig. 7(b) the results corresponding to the $L_z = 45$ Å QW of sample CT669. The isotropic conduction band shows a splitting that is similar to the bulk material. The Zeeman-splitting pattern for the valence band is, however, rather different from the one for bulk and also from the one for $B\|[001]$. In zero field, where the growth direction defines the quantization axis, the in plane g factor $g_\perp$ for the heavy-hole states vanishes. The heavy-hole doublet splits only due to the magnetic field induced moments. The in plane field mixes the light- and heavy-hole states belonging to the same irreducible representation. An anticrossing of the two Γ_4 states occurs around $B=2$ T. For the given QW the exchange energy is not large enough to reach a situation where the direction of the magnetic field is a good approximation for the quantization axis of the hole spins. Such a situation is reached for (Cd,Mn)Te/(Cd,Mg)Te QW's with smaller Δ and higher Mn content.[37] For the given QW a strong mixture of the heavy- and light-hole states is reached when the magnetization saturates. The good agreement of the model with the experiment is shown in Fig. 6 where we mark the calculated positions by arrows. The missing of a distinct peak for σ transition 3 and π transition 4 in the PLE spectra can be understood by calculating the relative size of the transition probabilities. They are proportional to the squares of the dipole matrix elements. The magnetic field dependence of the latter can be calculated once the eigenstates of the holes are determined. For the $L_z = 45$ Å well of sample CT669 the values are displayed in the inset of Fig. 6. They start from values close to 3 and 1 in zero field, the small deviations from the integer values which are exact for bulk material, are due to the lower symmetry of the QW potential. In agreement with the experiment the dipole matrix element for transition 3σ almost vanishes above $B=5$ T and the value for transition 4π is also rather small. Based on the calculations, it is also possible to identify the different transitions contributing to the Raman resonances shown in Fig. 5. The allowed scattering processes are shown in Fig. 7(b) and the corresponding energies are marked in Fig. 5. (We used the experimental energy values derived from the analysis of the PLE data.) As we plot the Raman intensities versus the energy of the incident light, a coincidence of the resonance maximum with the energy of the dipole transition from the initial state to the intermediate state is expected. The overall pattern of the resonance positions, i.e., the energy difference and polarizations, agree well with the observed PLE energies. The absolute values of the resonance positions are however below the PLE positions. We interpret this energy difference as the binding energy of the exciton at the neutral donor. Similar observations were made for resonances related to the $L_z = 20$ Å wide QW of sample CT669
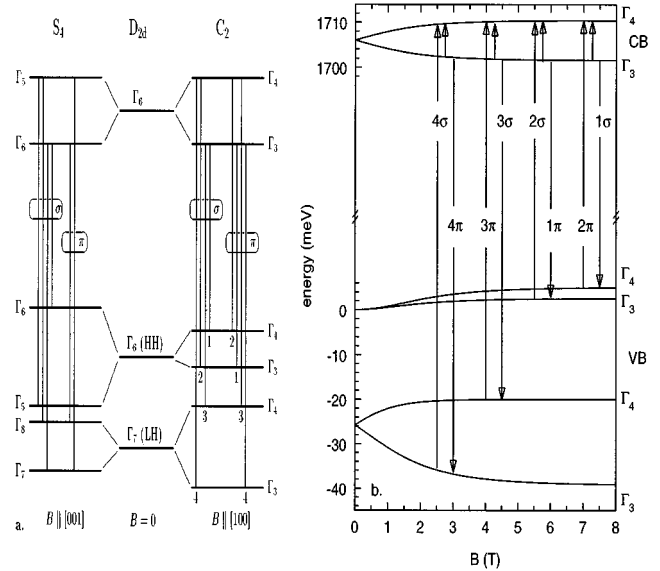
FIG. 7. (a) Schematic the level splitting for a semimagnetic quantum well under the influence of a magnetic field along the [001] and the [100] direction. The allowed electric-dipole transitions and their respective polarizations are shown. (b) Calculated Zeeman splitting of the lowest conduction and valence subbands for a $Cd_{0.97}Mn_{0.03}Te/Cd_{0.24}Mg_{0.76}Te$ single quantum well in an in plane magnetic field.

and of the $L_z = 45$ Å QW of sample CT671. The scattering in the binding energies for the D^0X complex may partly be caused by the different positions of the donors in the QW potential.

The assumption that neutral donors are already present in our MBE-grown samples is further supported by the excitation power dependence of the scattering efficiency which is linear over the range 0.02–20 W cm^{-2}. This is different from the undoped bulk material which tends to be p-type and donors are compensated. In this case the SFRS power dependence is nonlinear since neutral donors have to be created by the exciting photons.[39]

The knowledge of the relative size of the dipole matrix elements in conjunction with the cross section (8) can be used to estimate the width of the intermediate state involved in the scattering process. If only the resonant term in Eq. (8) is considered, the resonance profile is expected to have Lorentzian shape with an area

$$A \propto |\langle f|\vec{e}_S^*\vec{D}|l\rangle|^2 |\langle l|\vec{e}_I\vec{D}|i\rangle|^2/\Gamma_l. \qquad (14)$$

We introduced a finite width of the intermediate state by $E_l \rightarrow E_l + i\Gamma_l/2$. This result remains valid under the influence of inhomogeneous broadening, which does not affect the area under a resonance profile. The two $\sigma\pi$ resonances shown in Fig. 5 are determined with the same experimental configuration thus the unknown proportionality constant in Eq. (14) cancels when the areas are compared. We find an experimental ratio of 20:1 for the areas, which, when compared with the calculated ratio 3.2:0.3 of the numerators in Eq. (14), leads to a ratio of the homogeneous width of the

intermediate states of approximately 1:2. This value should be considered with some care, since our resonance profiles are not corrected for absorption, which is however a small effect for narrow SQW's.

V. CONCLUSION

We presented SFRS data for (Cd,Mn)Te/(Cd,Mg)Te QW's which provide a strong confinement of electrons and holes to a well consisting of a magnetic layer between non-magnetic barriers. The low-field data reveal an enhancement of the BMP effect caused by the QW localization. The observations can be explained by a modification of the BMP model used for bulk material and a variational solution of the QW-donor problem.

The symmetry reduction caused by an in plane magnetic field is clearly demonstrated by the occurrence of additional resonances in the Raman scattering cross section. The assignment of interband transitions to the resonances of the Raman processes is supported by model calculations of the magnetic field splitting of the subbands in in plane fields. The calculations reproduce the energies and the electric-dipole matrix elements between the mixed light-hole–heavy-hole states and the conduction band.

ACKNOWLEDGMENT

---

[*]Electronic address: dahl@physik.uni-wuerzburg.de

[1] R. E. Slusher, C. K. N. Patel, and P. A. Fleury, Phys. Rev. Lett. **18**, 77 (1967).

[2] D. G. Thomas and J. J. Hopfield, Phys. Rev. **175**, 1021 (1968).

[3] J. F. Scott, Rep. Prog. Phys. **43**, 951 (1980).

[4] S. Geschwind and R. Romestain, in *Light Scattering in Solids*, edited by M. Cardona and G. Güntherodt, Topics in Applied Physics Vol. 54 (Springer, Berlin, 1984).

[5] H. G. Häfele, in *Landau Level Spectroscopy*, edited by G. Landwehr and E. I. Rashba (Elsevier, Amsterdam, 1991), p. 579.

[6] V. F. Sapega, M. Cardona, K. Ploog, E. L. Ivchenko, and D. L. Mirlin, Phys. Rev. B **45**, 4320 (1992).

[7] V. F. Sapega, T. Ruf, M. Cardona, K. Ploog, E. L. Ivchenko, and D. L. Mirlin, Phys. Rev. B **50**, 2510 (1994).

[8] P. J. Boyce, J. J. Davies, D. Wolverson, K. Ohkawa, and T. Mitsuyu, Appl. Phys. Lett. **65**, 2063 (1994).

[9] D. Wolverson, P. J. Boyce, C. M. Townsley, B. Schlichtherle, and J. J. Davies, Proceedings of the 7th International Conference on II-VI Compounds and Devices [J. Cryst. Growth **159**, 229 (1996)].

[10] J. Furdyna and J. Kossut, *Diluted Magnetic Semiconductors*, Semiconductors and Semimetals Vol. 25 (Academic Press, Boston, 1988), p. 275; J. Furdyna, J. Appl. Phys. **64**, R29 (1988).

[11] M. Nawrocki, R. Planel, G. Fishman, and R. Galazka, Phys. Rev. Lett. **46**, 735 (1981).

[12] D. Heiman, P. A. Wolff, and J. Warnock, Phys. Rev. B **27**, 4848 (1983).

[13] D. L. Peterson, D. U. Bartholomew, U. Debska, A. K. Ramdas, and S. Rodriguez, Phys. Rev. B **32**, 323 (1985).

[14] P. A. Wolff, in *Diluted Magnetic Semiconductors* (Ref. 10), p. 413.

[15] D. L. Alov, S. I. Gubarev, and V. B. Timofeev, Zh. Éksp. Teor. Fiz. **86**, 1124 (1984) [Sov. Phys. JETP **59**, 658 (1984)].

[16] T. Dietl, M. Sawicki, M. Dahl, D. Heiman, E. D. Isaacs, M. J. Graf, S. I. Gubarev, and D. L. Alov, Phys. Rev. B **43**, 3154 (1991).

[17] M. Hirsch, R. Meyer, and A. Waag, Phys. Rev. B **48**, 5217 (1993).

[18] E.-K. Suh, D. U. Bartholomew, A. K. Ramdas, R. N. Bicknell, R. L. Harper, N. C. Giles, and J. F. Schetzina, Phys. Rev. B **36**, 9358 (1987).

[19] R. Meyer, M. Hirsch, G. Schaack, A. Waag, and R. N. Bicknell-Tassius, Superlatt. Microstruct. **9**, 165 (1991).

[20] D. Wolverson, J. J. Davies, S. V. Railson, M. P. Halsall, D. E. Ashenford, and B. Lunn, J. Cryst. Growth **138**, 656 (1994).

[21] M. P. Halsall, S. V. Railson, D. Wolverson, J. J. Davies, B. Lunn, and D. E. Ashenford, Phys. Rev. B **50**, 11 755 (1994).

[22] P. J. Klar, D. Wolverson, J. J. Davies, B. Lunn, D. E. Ashenford, and T. Henning, Proceedings of the 23rd International Conference on the Physics of Semiconductors, edited by M. Scheffler and R. Zimmermann (World Scientific, Singapore, 1996), p. 1485.

[23] R. Meyer, G. Schaack, and A. Waag, Mater. Sci. Forum **182-184**, 463 (1995).

[24] B. Kuhn-Heinrich, W. Ossau, T. Litz, A. Waag, and G. Landwehr, J. Appl. Phys **75**, 8046 (1994).

[25] B. Kuhn-Heinrich, W. Ossau, H. Heinke, F. Fischer, T. Litz, A. Waag, and G. Landwehr, J. Appl. Phys. Lett. **63**, 2932 (1993).

[26] J. Stühler, M. Hirsch, G. Schaack, and A. Waag, Phys. Rev. B **49**, 7345 (1994).

[27] Eunsoon Oh, A. K. Ramdas, N. Samarth, H. Luo, and J. K. Furdyna, Phys. Rev. B **47**, 7288 (1993).

[28] T. Dietl and J. Spałek, Phys. Rev. B **28**, 1548 (1983).

[29] R. L. Aggarwal, S. N. Jasperson, P. Becla, and R. R. Gałazka, Phys. Rev. B **32**, 5132 (1985).

[30] E. Molva and Le Si Dang, Phys. Rev. B **32**, 1156 (1985).

[31] C. Benoit la Guillaume, M. Combscot, and Yu. G. Semenov, *22nd International Conference on the Physics of Semiconductors*, edited by D. J. Lockwood (World Scientific, Singapore, 1995), p. 2481.

[32] G. Bastard, *Wave Mechanics Applied to Semiconductor Heterostructures* (Halsted Press, New York, 1988).

[33] W. Hayes and R. Loudon, *Scattering of Light by Crystals* (Wiley, New York, 1978).

[34] T. Z. Kachlishvili, Solid State Commun. **80**, 283 (1991).

[35] F. Neugebauer, J. Röseler, D. Suisky, and S. Rex, *21nd International Conference on the Physics of Semiconductors*, edited by P. Jiang and H.-Z. Zheng (World Scientific, Singapore, 1992), p. 748.

[36] P. Peyla, A. Wasiela, Y. Merle d'Aubign, D. E. Ashenford, and B. Lunn, Phys. Rev. B **47**, 3783 (1993).

[37] B. Kuhn-Heinrich and W. Ossau, Mater. Sci. Forum **182&184**, 491 (1995).

[38] J. A. Gaj, in *Diluted Magnetic Semiconductors* (Ref. 10), p. 288.

[39] S. I. Gubarev, T. Ruf, and M. Cardona, Phys. Rev. B **43**, 14 564 (1991).

[40] W. Ossau, U. Zehnder, B. Kuhn-Heinrich, A. Waag, T. Litz, and

G. Landwehr, Superlatt. Microstruct. **16**, 5 (1994).

[41] Y. R. Lee and A. K. Ramdas, Solid State Commun. **51**, 861 (1984).

[42] R. Romestain and C. Weisbuch, Phys. Rev. Lett. **45**, 2067 (1980).

[43] T. Friedrich, J. Kraus, M. Meininger, G. Schaack, and W. O. G. Schmitt, J. Phys. Condens. Matter **6**, 4307 (1994).

[44] S. Nakashima, T. Fukumoto, and A. Mitsuishi, J. Phys. Soc. Jpn. **35**, 1437 (1973).